The time between Paleolithic hearths

Ángela Herrejón-Lagunilla[1,2*], Juan José Villalaín[1], Francisco Javier Pavón-Carrasco[2,3], Mario Serrano Sánchez-Bravo[2,3], Santiago Sossa-Ríos[4], Alejandro Mayor[5], Bertila Galván[6], Ángel Carrancho[7**], Cristo M. Hernández[6,8**], Carolina Mallol[6,8,9**].

[1] Área de Física Aplicada, Departamento de Física, Universidad de Burgos; Burgos, Spain.

[2] Departamento de Física de la Tierra y Astrofísica, Facultad de Ciencias Físicas, Universidad Complutense de Madrid; Madrid, Spain.

[3] Departamento de Dinámica Terrestre y Observación de la Tierra, Instituto de Geociencias, Consejo Superior de Investigaciones Científicas-Universidad Complutense de Madrid; Madrid, Spain.

[4] Àrea de Prehistòria; Departament de Prehistòria, Arqueologia i Història Antiga, Facultat de Geografia i Història, Universitat de València; València, Spain.

[5] Àrea de Prehistòria, Departament de Prehistòria, Arqueologia, Història Antiga, Filologia Llatina i Filologia Grega, Facultat de Filosofia i Lletres, Universitat d'Alacant; Sant Vicent del Raspeig, Spain.

[6] Área de Prehistoria, Unidad de Docencia e Investigación de Prehistoria, Arqueología e Historia Antigua, Departamento de Geografía e Historia, Facultad de Humanidades, Universidad de La Laguna; San Cristóbal de La Laguna, Tenerife, Spain.

[7] Área de Prehistoria, Departamento de Historia, Geografía y Comunicación, Universidad de Burgos; Burgos, Spain.

[8] Archaeological Micromorphology and Biomarkers Laboratory, Instituto Universitario de Bio-Orgánica Antonio González, Universidad de La Laguna; San Cristóbal de La Laguna, Tenerife, Spain.

[9] Department of Anthropology, University of California, Davis, California, United States.

*Corresponding author. Email: aherrejon@ubu.es; anherrej@ucm.es; angelaherrejonlagunilla@gmail.com

**Equal contribution

Resolving the timescale of human activity in the Paleolithic is one of the most challenging problems in prehistoric archeology. The duration and frequency of hunter-gatherer camps reflects key aspects of social life and human-environment interactions. However, the time dimension of Paleolithic contexts is generally inaccurately reconstructed due to the limitations of dating techniques[1], the impact of disturbing agents on sedimentary deposits[2], and the palimpsest effect[3-4]. Here, we report high-resolution time differences between six Middle Paleolithic hearths from El Salt Unit X (Spain) obtained through archeomagnetic and archeostratigraphic analyses. The set of hearths represents at least ~200-240 years with 99% probability, with decade and century-long intervals between the different hearths. Our results provide a quantitative estimate of the time framework for the human occupation events included in the studied sequence. This is a step forward in Paleolithic archeology, a discipline in which human behavior is usually approached from a temporal scale typical of geological processes, while significant change may happen at the smaller scales of human generations. Here, we reach a time scale close to a human lifespan.

While it has been hypothesized that Paleolithic hunter-gatherers were highly mobile, key aspects of their lifestyle, such as the time between camps and the size of traveling groups, remain unclear. Complexity in the formation of Paleolithic sites make it difficult to single out human occupation episodes and resolve the time between them. Yet, models based on cross-cultural comparisons predict that the timing and duration of hunter-gatherer camps and of the activities carried out in them may be conditioned by seasonal cycles, the distribution of raw materials, diet, ritual, and other such natural and cultural factors, and that their interplay results in settlement and mobility patterns recognizable in the archeological record[5-6]. Narrowing down the timescales of the Paleolithic to a degree of resolution sufficiently high to test these models remains a challenging problem for different reasons. Absolute dates for archeological contexts beyond the limits of radiocarbon dating around 50-60 ka are imprecise and other techniques like OSL, TL, etc. usually have a resolution that is far from the scale of human life (with error ranges of several thousand years)[1]. Thus, the chronometric dates associated with Paleolithic contexts entail error ranges on the order of millennia, far beyond the scale of a human lifespan. Further, the natural processes affecting Paleolithic sedimentary deposits through time normally disturb and disorder the original sequence of events[2], and the palimpsest effect[3-4 (and references therein)] lumps archeological evidence from different time periods into a single apparent surface. Aside from behavioral models focusing on mobility, the patent temporal and spatial distortion of the Paleolithic archeological record also prevents us from testing other longstanding demographic, ecological and structural models on hunter-gatherer societies that require accurate estimates on group and population size, environmental conditions, and the use of space[7-12].

Recent interdisciplinary efforts have provided high temporal and spatial resolution at a few Middle and Upper Paleolithic sites, elucidating patterns of hunter-gatherer group mobility at a scale of seasons and decades based on the identification of speleothem formation cycles associated with human occupations[13-15] and Sr isotope ratios on human tooth specimens[16]. However, there is a need for methods applicable to a broader range of materials and contexts and with the potential to aid in palimpsest dissection, allowing for time-resolved behavioral analysis of archeological remains. Within this framework, archeological hearths stand out as direct transmitters of technological and behavioral information, as well as spatial markers of human living surfaces. Previous multi-scalar, interdisciplinary investigations of Middle Paleolithic hearths from El Salt Unit X (ca. 52 ka BP), in Spain[17-18], have revealed significant temporal separations between the remains from white layers (mainly woody ash and other combustion remains) and black layers (thermally altered substrate above which the fire was made) of single hearths. Additionally, temporal separations among the black layers of different hearths resting on a single apparent surface have also been verified [19-22]. Albeit contributing to palimpsest dissection, the results of these studies approach time at an imprecise, relative scale inferred from lithic technology, sedimentary accretion, and soil formation. Quantitative approaches to the human timescale are called for.

Archeomagnetic analysis of burnt materials and sedimentary combustion features has been previously used for temporal contextualization in Middle Paleolithic contexts[23-25]. The ferromagnetic minerals (*s.l.*) contained in burnt materials are potential recorders of the Earth's magnetic field (EMF) direction through the acquisition of thermoremanence (>600 ºC) or partial thermoremanence. In turn, the direction of the EMF steadily changes a few degrees over time at the regional scale due to the phenomenon of Secular Variation (SV). For mid-latitude areas as the Iberian Peninsula, the amplitude of angular variation is about ± 25º in declination while the inclination oscillates between 40º to 70º [26]. Hence, statistically significant deviations between mean archeomagnetic directions among different archeological hearths exposed on the same excavation surface or included in the same sedimentary deposit suggest that adjacent hearths may not being contemporaneous. Comparison of the observed angular deviations with the variations inferred from paleomagnetic reconstructions of the EMF in the past can be used to infer minimum elapsed times between the burning of the different fires[23]. It is important to note that synchrony cannot be inferred for two main reasons. First, the erratic nature of the SV directional changes and their confinement within the previously mentioned range of variation implies that the same direction of the EMF can recur multiple times over time. Second, there are statistical uncertainties associated with the calculated mean directions. However, synchrony can be ruled out if the directions are clearly distinguishable.

Although the aforementioned studies on Paleolithic hearths have explored this approach[23-25], our knowledge on regional SV curves and global paleomagnetic trends has significantly increased (e.g. [26-30]) since previous attempts at inferring quantitative temporal estimates based solely on directional data from Middle Paleolithic hearths[23]. Furthermore, the high potential of hearth black layers to record EMF directions has been highlighted: recent experimental archeomagnetic data obtained from a set of 5-year-old open air hearths showed that the black layers preserved reliable EMF directions despite the occurrence of processes including weathering and bioturbation[31]. On this basis, we propose an estimate of the minimum time (with certain probability) involved in the formation of a set of six archeological hearths from El Salt Unit X using recent paleomagnetic reconstructions and archeostratigraphic analyses.

El Salt Unit X

El Salt [Alcoi, Alacant, Spain (38.6869º N, 0.5090º W); Fig. 1 and Extended data Fig. 1; Supplementary Note 1] is a key site for the study of Neandertals due to its rich, well-preserved archeological and organic-rich sedimentary record, including biomolecules[20, 32-33]. It comprises a 4-meter-thick open-air deposit at the foot of a 40-meter tall limestone cliff. Unit X has been dated by thermoluminescence to ca. 52 ka BP[17] and has been divided into an upper sandy Subunit Xa, and a lower slightly clayier Subunit Xb. Unit X exhibits a complex internal stratification of discontinuous sedimentary facies, locally bioturbated in-situ hearths (white-black layer successions; Extended data Fig. 2) and beds of archeological material[34-36]. This complexity is particularly evident near the back wall ("Inner Part", Extended data Figs. 1 and 3). Unit X was excavated with emphasis on facies distinction. All archeological remains were collected through three dimensional mapping and separated according to the sedimentary facies in which they were found. The results of subsequent microstratigraphic geoarcheological investigations were used to assess the degree of integrity of the Unit X archeological assemblages[19-20]. We selected six well-preserved in-situ hearths: one is from Subunit Xa (H34) and five are from Subunit Xb (H48, H50, H55, H57 and H59) (Extended data Fig. 4). The latter have been tentatively correlated with archeological remains following stratigraphic superposition criteria (Extended data Fig. 5). Oriented blocks of sediment from the selected hearths were collected to measure their archeomagnetic signal and estimate the time between them (further details in Methods section).

Ordering the hearths sequence

Careful excavation of El Salt unit Xb enabled the field identification of ten layers of archeological remains and their tentative correlation with various hearths (Methods; Extended data Fig. 5). These layers were individualized considering microtopographic features and stratigraphic relationships among the material remains [cf. [37]]. Archeostratigraphic analysis of the material remains (Supplementary Note 2) provided critical data regarding temporal sequencing of the hearths. H34 (in Subunit Xa) clearly overlies the other hearths. It is stratigraphically separated from the others by mm-to-cm-thick layers of sediment. Archeostratigraphic analysis of the Unit Xb hearths shows that their stratigraphic order, from top to bottom, is: H57, H55, H48, H59 and H50 (Figs. 1 and Extended data Fig. 5) [For details see Supplementary Note 2].

Estimating the time between the hearths

Once the sequence of hearths was determined, archeomagnetism was used to estimate, with a certain probability, the minimum time that had passed between their respective burning events. This estimation was based on a detailed assessment of the archeomagnetic signals recorded in the hearths. Rock magnetic experiments show that magnetite (in some cases, slightly oxidized) is the main ferromagnetic mineral present (Curie temperatures close to 585-600 ºC; Extended data Fig. 6). Differences in the reversibility of the thermomagnetic curves between hearth layers indicate variable thermal impacts. The highest temperatures were recorded in white layers, which represent wood ash and other combustion residues, while the hearth substrates (black layers) recorded lower temperatures (Supplementary Note 3). This stratigraphic coherence has been previously observed in experimental contexts[31].

The mean archeomagnetic directions were obtained through stepwise thermal demagnetization of the natural remanent magnetization (NRM) of oriented specimens (Table 1; Extended data Fig. 7). Only mean directions that meet minimum quality criteria ($N>6$, $k>50$, $\alpha_{95}<10º$) have been considered for the temporal calculations. Consequently, H57 was not included in the analysis. The main mechanism involved in the magnetization of the black layers of the hearths, which are our main focus due to their high potential for recording accurate archeomagnetic directions [31], was partial thermoremanence (pTRM). Thus, the black layers' pTRM represents the characteristic remanent magnetization (ChRM) related to the time of the last combustion event.

The ChRM direction was isolated between 150-250 ºC and 330-550 ºC (Extended data Fig. 8), with higher temperature steps representing the record prior to the last burning. In some cases, maximum unblocking temperatures of the ChRM direction reached 575-600 ºC, indicating full thermoremanence (TRM) or thermochemical magnetization (TCRM). The record occurs during the initial cooling, which indicates that directional record is reliable[38]. Differences in the maximum unblocking temperatures of the ChRM direction are coherent with the expected variability of heat distribution in simple open hearths[39]. Demagnetized specimens commonly show an abrupt drop around 250-300 ºC in NRM decay plots followed by a smoother decrease (e.g. Extended data Fig. 8a). Detailed information about the specimens' selection criteria for the calculation of the mean directions is provided in the Supplementary Methods 1.

To estimate the minimum elapsed time, denoted as Δt_{min}, between two directions recorded for each pair of hearths, we relied on reference Paleosecular Variation Curves (PSVCs) at El Salt coordinates given by two different paleomagnetic reconstructions: SHA.DIF.14k[27] and ARCHKALMAG14k[28]. These curves cover the last 14,000 years and are exclusively based on TRM data, representing snapshots readings of the EMF. Despite not reaching the ages of the target hearths, there are two compelling reasons for their use: (1) due to data scarcity, only one EMF continuous reconstruction covers a pre-Holocene time span[40] and it lacks the necessary accuracy for pre-Holocene times due to uncertainties in dating and the materials used for obtaining the paleomagnetic data; (2) the hearths belong to a period marked by EMF stability, allowing us to assume that the SV behavior during the last millennia is comparable to that of the age of the materials under study.

First, the Probability Density Function (PDF) of the angular deviation between the given directions of each pair of hearths was calculated by combining both Fisherian directions[41], considering their declination/inclination and their associated error α_{95} (Supplementary Methods

2) (e.g. Fig. 2b). Next, we obtained the PDF of the minimum elapsed time (Δt_{min}) from the directional PSVC for a range of critical angular deviations (Ω_c) spanning from 1º to 25º in 1º increments (Supplementary Methods 2). To get the PDF for each individual angular deviation (Ω_c), we explored all possible combinations of pairs of directional data using the chosen PSVC, calculating the minimum time intervals required to achieve the critical value Ω_c within the designated time frame (e.g. Fig. 2c). This step was repeated using the PSVCs of the two paleoreconstructions (Fig. SM2.4 in Supplementary Methods 2). Finally, we combined the PDF of the angular deviation between each pair of hearths (Fig. 2b) with each PDF of the minimum elapsed time for the set of critical values of Ω_c (Fig. 2c). This resulted in a new PDF (e.g. Fig. 2d) that contains the probability of the minimum elapsed time (Δt_{min}) between the chosen pair of directional archeomagnetic data. The probability for Δt_{min} is provided in terms of the most often value (i.e. mode) or 68%, 95% or 99% confidence levels. The entire procedure was applied to each pair of successive hearths, following the temporal order determined by archeostratigraphic analyses. The main results of the calculations are presented in Fig. 3, in the Extended data Table 1, and Fig. SM2.10 of the Supplementary Methods 2. Temporal inferences have similar magnitude regardless of the archeomagnetic model used. To assess the robustness of the results, we created a set of synthetic PSVCs, referred to as "*toy-model*", based on the temporal characteristics of ARCHKALMAG14k at El Salt coordinates. We then applied the same approach to this *toy-model* and obtained results were similar to those produced by the selected paleoreconstructions (Supplementary Methods 2). Several tests to validate the method are included in Supplementary Methods 3.

This approach allows to estimate the minimum elapsed time necessary to account for the angular deviation observed between the hearths in each pair. This time frame varies from several decades to over a century at the considered confidence levels. Inherent variability in archeomagnetic data may contribute to time overestimation, so the method should not be applied to coeval records. Our study takes into account stratigraphic constraints, such as the superimposition of some structures on others, suggesting that some time may have indeed passed between fires.

As expected, the smallest minimum elapsed times (Fig. 3) correspond to fires whose directions (considering the α_{95}) present lower angular deviation (i.e., H34-H55 and H55-H48, with most probable angular deviations of 6.3º and 6.8º, respectively; Fig. SM2.1 in Supplementary Methods 2). The largest angular deviations are found for the pairs H48-H49 (most probable angular deviation = 12.5º; Fig. SM2.1 in Supplementary Methods 2) and H59-H50 (most probable angular deviation = 13.0º; Fig. SM2.1 in Supplementary Methods 2), and thus they are associated with higher minimum elapsed times (see detailed results in Figures E10 in Supplementary Methods 2 and Extended Data Table 1).

The H34-H55 and H55-H48 pairs exhibit partially overlapped α_{95} values (Fig SM2.10 in Supplementary Methods 2). In absence of archeostratigraphic constrains, this would suggest that complete exclusion of synchrony cannot be confirmed. However, certain amount of time must have passed between H34 and H55 because they belong to different stratified sedimentary layers (subunit Xa and Xb, respectively). The small angular deviation between H34 and H55 could indeed reflect a genuine change in the EMF direction. Our calculations suggest that the time lag between these two structures is 25 yrs (99% confidence level), 50-60 yrs (95%) and 140-220 yrs (68%) and 105 to 120 yrs (mode). Mode and 68% tend to overestimate the minimum elapsed times, while the 99% is the most conservative result in terms of minimum times (see Supplementary Methods 3 for more details). Thus, at least 25 yrs may separate H34 and H55. In the case of H55-H48, they belong to the same stratigraphic subunit (Xb). There is a significant overlap in their α_{95}, and consistently, our results consistently indicate the shortest time lag for this pair of hearths, with a range of 20-25 yrs (99%), 45-55 yrs (95%), 145-230 yrs (68%) and 95-105 yrs (mode). The superposition of H55-H48 determined by archeostratigraphic inferences suggest that a certain time span could have existed. Considering the 99%, H55-H48 are at least 25 years apart.

The data for hearths H48 and H59 (both from subunit Xb) indicates that the minimum time required to account for the observed angular deviation between their directions falls within the range of 70-85 yrs (99%), 135-175 yrs (95%), 440-595 yrs (68%) or 235-345 yrs (mode).

Assuming the most conservative result (99%), a minimum of 70-85 years separate these two hearths. The oldest pair of directional data (H59-H50, both from subunit Xb) provides similar results, with a minimum elapsed time ranging from 85-105 yrs (99%) 160-205 yrs (95%), 505-650 yrs (68%) or 280 to 400 yrs (mode). These two structures exhibit the greatest temporal difference, reaching up to a century approximately (99%).

According to our temporal estimations and considering the most conservative results (99% confidence level), the entire hearth sequence, along with associated sediments and materials, was formed over a minimum time span of ~200-240 yrs (Fig. 3). It suggests that several centuries were required for the complete formation of the sequence.

Archeological implications

The results of this study allowed us to assign a minimum time frame between the hearths on a human generational timescale. These new data support the idea that archeological palimpsests can be investigated at a decadal and centennial temporal resolutions, further advancing the study of Neanderthal societies. This provides an opportunity to compare and explore behavioral and paleoenvironmental changes among hearth-related assemblages separated by a known time spans. This advancement brings us closer to the possibility of modelling Paleolithic hunter-gatherer behavior and empirically addressing long-standing debates.

This study also highlights the potential of our method to resolve the timescale of human activity in other archeological contexts with in-situ combustion features from any period and region. The proposal is suitable for any archeological context if the hearths (*1*) represent in-situ burning, (*2*) have not suffered severe mechanical alterations that may have disturbed the directional record and (*3*) the record did not take place in a moment of instability of the EMF (polarity transitions or geomagnetic excursions). The proposal is of special interest for the oldest contexts (i.e., Paleolithic), where the error ranges of absolute dates are normally in the order of thousands of years.

Main references

1. S. E. Trumbore, "Radiocarbon geochronology" in Quaternary geochronology: Methods and applications, J. Stratton Noller, J. M. Sowers, W. R. Lettis, Eds. (AGU, 2000), vol. 4, pp. 41-60.

2. P. Karkanas, P. Goldberg, Reconstructing archaeological sites: Understanding the geoarchaeological matrix (Wiley, 2018).

3. G. Bailey, Time perspectives, palimpsests and the archaeology of time. Journal of Anthropological Archaeology 26, 198-223 (2007).

4. C. Mallol, C. M. Hernández, Advances in palimpsest dissection. Quaternary International 417, 1-2 (2016).

5. L. R. Binford, Willow smoke and dogs' tails: hunter-gatherer settlement systems and archaeological site formation. American Antiquity 45, 4-20 (1980).

6. R. L. Kelly, Hunther-gatherer mobility strategies. Journal of Anthropological Research 39 (3), 277-306 (1983).

7. R. L. Bettinger, R. Garvey, S. Tushingham, Hunter-gatherers: archaeological and evolutionary theory (Springer, 2015).

8. M. J. Hamilton, B. T. Milne, R. S. Walker, J. H. Brown, Nonlinear scaling of space use in human hunter–gatherers. Proc. Natl. Acad. Sci. U.S.A. 104, 4765-4769 (2007).

9. M. J. Hamilton, B. T. Milne, R. S. Walker, O. Burger, J. H. Brown, The complex structure of hunter–gatherer social networks. Proceedings of the Royal Society B: Biological Sciences, 274, 2195-2203 (2007).

10. P. Draper, Crowding among hunter-gatherers: The !Kung bushmen. Science 182, 301-303 (1973).

11. C. R. Ember, Residential variation among hunter-gatherers. Behavior Science Research 10, 199-227 (1975).

12. B. Winterhalder, W. Baillargeon, F. Cappelletto, I. R. Daniel Jr, C. Prescott, The population ecology of hunter-gatherers and their prey. Journal of Anthropological Archaeology 7, 289-328 (1988).

13. S. Vandevelde, J. E. Brochier, C. Petit, L. Slimak, Establishment of occupation chronicles in Grotte Mandrin usingm sooted concretions: Rethinking the Middle to Upper Paleolithic transition. Journal of Human Evolution 112, 70-78 (2017).

14. S. Vandevelde, J. L. Lacour, C. Quéré, L. Marie, C. Petit, L. Slimak, Identification du rythme annuel de précipitation des carbonates pariétaux pour un calage micro-chronologique des occupations archéologiques pyrogéniques: cas de la Grotte Mandrin (Malataverne, Drôme, France). BSGF - Earth Sciences Bulletin 192, 1-22 (2021).

15. L. Slimak, C. Zanolli, T. Higham, M. Frouin, J. L. Schwenninger, L. J. Arnold, M. Demuro, K. Douka, N. Mercier, G. Guérin, H. Valladas, P. Yvorra, Y. Giraud, A. Seguin-Orlando, L. Orlando, J. E. Lewis, X. Muth, H. Camus, S. Vandevelde, M. Buckley, C. Mallol, C. Stringer, L. Metz, Modern human incursion into Neandertal territories 54,000 years ago at Mandrin, France. Science Advances 8, eabj9496 (2022).

16. F. Lugli, A. Nava, R. Sorrentino, A. Vazzana, E. Bortolini, G. Oxilia, S. Silvestrini, N. Nannini, L. Bondioli, H. Fewlass, S. Talamo, Tracing the mobility of a Late Epigravettian (~ 13 ka) male infant from Grotte di Pradis (Northeastern Italian Prealps) at high-temporal resolution. Scientific Reports 12, 1-13 (2022).

17. B. Galván, C. M. Hernández, C. Mallol, N. Mercier, A. Sistiaga, V. Soler, New evidence of early Neandertal disappearance in the Iberian Peninsula. Journal of Human Evolution 75, 16-27 (2014).

18. M D. Garralda, B. Galván, C. M. Hernández, C. Mallol, J. A. Gómez, B. Maureille, Neandertals from El Salt (Alcoy, Spain) in the context of the latest Middle Palaeolithic populations from the southeast of the Iberian Peninsula. Journal of Human Evolution 75, 1-15 (2014).

19. C. Mallol, C. M. Hernández, D. Cabanes, A. Sistiaga, J. Machado, A. Rodríguez, L. Pérez, B. Galván, The black layer of Middle Palaeolithic combustion structures. Interpretation and archaeostratigraphic implications. Journal of Archaeological Science 40, 2515-2537 (2013).

20. L. Leierer, M. Jambrina-Enríquez, A. V. Herrera-Herrera, R. Connolly, C. M. Hernández, B. Galván, C. Mallol, Insights into the timing, intensity and natural setting of Neandertal occupation from the geoarchaeological study of combustion structures: A micromorphological and biomarker investigation of El Salt, unit Xb, Alcoy, Spain. PLoS ONE 14, e0214955 (2019).

21. A. Mayor, C. M. Hernández, J. Machado, C. Mallol, B. Galván, On identifying Palaeolithic single occupation episodes: archaeostratigraphic and technological approaches to the Neandertal lithic record of stratigraphic unit Xa of El Salt (Alcoi, eastern Iberia). Archaeological and Anthropological Sciences 12, 84 (2020).

22. J. Machado, F. J. Molina, C. M. Hernández, A. Tarriño, B. Galván, Using lithic assemblage formation to approach Middle Palaeolithic settlement dynamics: El Salt Stratigraphic Unit X (Alicante, Spain). Archaeological and Anthropological Sciences 9, 1715–1743 (2017).

23. R. Sternberg, E. H. E. Lass, "An Archaeomagnetic Study of Two Hearths from Kebara Cave, Israel" in Kebara Cave, Mt. Carmel, Israel. The Middle and Upper Palaeolithic Archaeology. Part I (American School of Prehistoric Research Bulletins 49, 2007), pp. 123-130.

24. Á. Carrancho, J. J. Villalaín, J. Vallverdú, E. Carbonell, Is it possible to identify temporal differences among combustion features in Middle Palaeolithic palimpsests? The archaeomagnetic evidence: A case study from level O at the Abric Romaní rock-shelter (Capellades, Spain). Quaternary International 417, 39-50 (2016).

25. C. Zeigen, R. Shaar, Y. Ebert, E. Hovers, Archaeomagnetism of burnt cherts and hearths from Middle Palaeolithic Amud Cave, Israel: Tools for reconstructing site formation processes and occupation history. Journal of Archaeological Science 107, 71-86 (2019).

26. A. Molina-Cardín, S. A. Campuzano, M. L. Osete, M. Rivero-Montero, F. J. Pavón-Carrasco, A. Palencia-Ortas, F. Martín-Hernández, M. Gómez-Paccard, A. Chauvin, S. Guerrero-

Suárez, J. C. Pérez-Fuentes, G. McIntosh, G. Catanzariti, J. C. Sastre Blanco, J. Larrazabal, V. M. Fernández Martínez, J. R. Álvarez Sanchís, J. Rodríguez-Hernández, I. Martín Viso, D. Garcia i Rubert, Updated Iberian Archeomagnetic Catalogue: New Full Vector Paleosecular Variation Curve for the Last Three Millennia. Geochemistry, Geophysics, Geosystems 19, 3637–3656 (2018).

27. F. J. Pavón Carrasco, M. L. Osete, J. M. Torta, A. De Santis, A geomagnetic field model for the Holocene based on archaeomagnetic and lava flow data. Earth and Planetary Science Letters 388, 98-109 (2014).

28. M. Schanner, M- Korte, M. Holschneider. ArchKalmag14k: A Kalman-Filter Based Global Geomagnetic Model for the Holocene. Journal of Geophysical Research: Solid Earth, 127: e2021JB023166 (2022).

29. C. Constable, M. Korte, S. Panovska, Persistent high paleosecular variation activity in southern hemisphere for at least 10000 years. Earth and Planetary Science Letters 453: 78-86 (2016).

30. M.L. Osete, A. Molina-Cardín, S.A. Campuzano, G. Aguilella-Arzo, A. Barrachina-Ibañez, F. Falomir-Granell, A. Oliver Foix, M. Gómez-Paccard, F. Martín-Hernández, A. Palencia-Ortas, F.J. Pavón-Carrasco, M. Rivero-Montero, Two archaeomagnetic intensity maxima and rapid directional variation rates during the Early Iron Age observed at Iberian coordinates. Implications on the evolution of the Levantine Iron Age Anomaly. Earth and Planetary Science Letters 533, 116047 (2020).

31. Á. Herrejón Lagunilla, Á Carrancho, J. J. Villalaín, C. Mallol, C. M. Hernández, An experimental approach to the preservation potential of magnetic signatures in anthropogenic fires. PLoS ONE 14 (8), e0221592 (2019).

32. A. Sistiaga, C. Mallol, B. Galván, R. E. Summons. The Neandertal Meal: A New Perspective Using Faecal Biomarkers. PLoS ONE 9 (6): e101045 (2014).

33. L. Leierer, Á. Carrancho Alonso, L. Pérez, Á. Herrejón Lagunilla, A. V. Herrera-Herrera, R. Connolly, M. Jambrina-Enríquez, C. M. Hernández Gómez, B. Galván, C. Mallol, It's getting hot in here – Microcontextual study of a potential pit hearth at the Middle Paleolithic site of El Salt, Spain. Journal of Archaeological Science 123: 105237 (2020).

34. B. Galván, El Salt (Alcoi, Alicante): estado actual de las investigaciones. Recerques del Museu D'Alcoi 1, 73-80 (1992).

35. M. P. Fumanal García, El yacimiento musteriense de El Salt (Alcoi, País Valenciano). Rasgos geomorfológicos y climatoestratigrafía de sus registros. SAGVNTVM 27, 39-55 (1994).

36. B. Galván, C. M. Hernández, C. Mallol, J. Machado, A. Sistiaga, F. J. Molina, L. Pérez, R. Afonso, M. D. Garralda, N. Mercier, J. V. Morales, A. Sanchís, A. Tarriño, J. A. Gómez, A. Rodríguez, I. Abreu, P. Vidal, "El Salt. The Last Neandertals Of The Alicante Mountains (Alcoy, Spain)" in Pleistocene and Holocene hunter-gatherers in Iberia and the Gibraltar strait: the current archaeological record, R. Sala, Ed., E. Carbonell. J. M. Bermúdez de Castro, J. L. Arsuaga, Coords. (Fundación Atapuerca, Servicio de Publicaciones de la Universidad de Burgos, 2014), pp. 380-388.

37. J. Machado, L. Pérez, Temporal frameworks to approach human behaviour concealed in Middle Palaeolithic palimpsests: A high-resolution example from El Salt Stratigraphic Unit X (Alicante, Spain). Quaternary International 417, 66-81 (2016).

38. D. J. Dunlop, Ö. Özdemir, Rock Magnetism. Fundaments and frontiers. (Cambridge University Press, 1997).

39. Á. Carrancho, J. J. Villalaín, Different mechanism of magnetisation recorded in experimental fires: Archaeomagnetic implications. Earth and Planetary Science Letters, 312, 176-187. (2011)

40. S. Panovska, C. G. Constable, M. Korte, Extending global continuous geomagnetic field reconstructions on timescales beyond human civilization. Geochemistry, Geophysics, Geosystems, 19(12), 4757-4772. (2018).

41. R. Fisher, Dispersion on a Sphere Author. Proceedings of the Royal Society of London. Series A, Mathematical and Physical Sciences, 217 (1130), 295-305 (1953).

42. P. Wessel, J. F. Luis, L. Uieda, R. Scharroo, F. Wobbe, W. H. F. Smith, D. Tian, The Generic Mapping Tools version 6. Geochemistry, Geophysics, Geosystems, 20, 5556–5564 (2019).

Tables

Table 1. Mean archeomagnetic directions of the studied hearths along with their respective statistical parameters, following Fisher statistics[41]. N = number of specimens used to calculate the mean direction; N' = total number of thermally demagnetized specimens; Dec. (º) = declination; Inc. (º) = inclination; *k* = precision parameter; α_{95} (º) = semi angle of confidence cone at 95% probability (p = 0.05). Thermal demagnetization of Natural Remanent Magnetization (NRM) is performed only once on each specimen due to the irreversible character of the experiment (it causes the progressive destruction of the original NRM). For this reason, a minimum of 8 specimens per hearth were analyzed to obtain mean archaeomagnetic directions.

Figures

Fig. 1. Plane layout and cross-sections representing the relative position of all the materials from El Salt stratigraphic subunit Xb studied in this paper. (A) Plane layout of the excavation area (grey zones indicate the location of C, D, and E). (B) North-West-to-South-East cross-section, plotting the position of all the archeological materials. (C-E) Individualized cross-sections relating to the selected hearths: North-East-to-South-West cross-section representing H55, H57 and their stratigraphically associated layers of archeological remains (C); North-West-to-South-East cross-section representing H48, H50 and their stratigraphically associated layers of archeological remains (D); and West-to-East cross-section representing H48, H59 and their stratigraphically associated layers of archeological remains (E). Map of Iberia has been custom-made with Generic Mapping Tools[42].

Fig. 2. Example of time estimation steps using the mean directions of H50 and H59 and SHA.DIF.14k reconstruction[27]. (A) Equal area projection with the mean archeomagnetic directions of H50 (green; 9 specimens from 1 oriented block) and H59 (red; 8 specimens from 1 oriented block) based on Fisher's statistics[41]. Most intensely colored symbols represent the mean

directions and their respective semi angle α_{95} (confidence cone at 95% probability; p=0.05). Lighter-colored points represent the directions of individual specimens. Thermal demagnetization of Natural Remanent Magnetization (NRM) is performed only once on each specimen due to the irreversible character of the experiment (it causes the progressive destruction of the original NRM). For this reason, a minimum of 8 specimens per hearth were demagnetized to obtain directional data. Specimens shown here correspond to those accepted after filtering (Supplementary Methods 1). (B) Probability Density Function (PDF) of the angular deviation between H59 and H50 directions (considering their respective α_{95}), calculated considering a sampling of 10^8 pairs of directions. (C) Some examples of PDF of the minimum elapsed time (Δt_{min}) for different critical angles (Ω_C) according to the SHA.DIF.14k paleomagnetic reconstruction. These PDFs are based on the histograms shown Fig. SM2.4a (Supplementary Methods 2; total number of pairs of directions considered for the histograms: 27454 pairs for Ω_C=5º; 25298 pairs for Ω_C=10º; 21059 pairs for Ω_C=15º; 14343 pairs for Ω_C=20º; 7401 pairs for Ω_C=25º). (D) Combined probability density function of the PDF of the angular distance between the two hearths (A) and the PDF of the Δt_{min} for different Ω_C according to SHA.DIF.14k. The purple, red, green and orange lines represent the Δt_{min} with 99% confidence level, 95% confidence level, 68% confidence level and mode, respectively (i.e. the minimum elapsed time to explain the angular deviation between H59 and H50 mean directions at a given probability).

Fig. 3. Sequence of the studied hearths ordered according to archeostratigraphic inferences, along with the minimum temporal differences (99% confidence level, 95% confidence level, 68% confidence level and mode) between consecutive structures, as inferred from the archeomagnetic data. The shown intervals reflect the differences in the estimated minimum elapsed time regarding the paleoreconstruction used. The hearth at the top of the figure (H34) is the most superficial in the studied sequence, while the hearth at the bottom (H50) is the deepest. The limits of the time elapsed between each pair of hearths are determined by the different values provided by the three paleomagnetic reconstructions used.

Methods

Studied hearths

El Salt Unit X contains a substantial quantity of archeological remains (Extended data Fig. 3), including hearths. However, not all of these hearths were suitable for sampling in this study. In some cases, the hearths were too small to obtain sufficient material for archeomagnetic experiments. In other instances, two or more hearths physically overlapped and could not be individually sampled, which poses problems for archeomagnetic analyses due to standard size of cubic specimens (~ 2 cm sides) used in these studies., Additionally, preservation quality is crucial, and signs of post-depositional mechanical disturbances in the structures can lead to unreliable archeomagnetic results, as discussed in detail elsewhere[43].

Any structures that exhibited macroscopic signs of disturbance or bioturbation, such as facies discontinuity, were excluded from sampling. Ultimately, we selected six hearths: H34, H48, H50, H55, H57 and H59. All of these hearths belong to subunit Xb (Extended data Fig. 4), except for H34, which corresponds to Subunit Xa. Their associated archeological assemblages underwent archeostratigraphic analyses, as discussed in the next section. H57 and H55 are located in the Inner Part of the site, while H48, H50 and H59 are situated in the Outer Part (Fig. 1a).

Archeomagnetic analyses

Archeomagnetic investigations at El Salt have been conducted continuously since 2014, with the exception of the the 2020 season due to the COVID19 pandemic. Among various materials, we collected 13 oriented blocks with burnt sedimentary facies from the mentioned hearths: 2 from H34, 1 from H48, 4 from H50, 4 from H55, 1 from H57, and 1 from H59. These magnetically oriented monoliths of sediment had a depth of ~ 5-6 cm, with the most heated surface at the top. The number of blocks collected depended on the size of the exposed burnt surface, taking into account that other samples were also collected for complementary techniques such as soil micromorphology, mineralogy (FTIR) or biomarkers, among others.

Most blocks contained mainly the black layer facies on top, which represents the thermally altered substrate on which the fire was made, although occasionally white layers (mainly wood ash and other combustion residues) were also present in some of them. In some cases, consolidation with waterglass (Sodium silicate + water) was necessary before conducting the laboratory analyses. Afterwards, the blocks were cut into cubic specimens (~8-10 cm^3) carefully keeping the orientation lines. A total of 105 oriented specimens were processed. Previous investigations performed on experimental open-air hearths similar to those studied here and using the same sampling techniques showed that the observed errors in direction can be considered stochastic and that no statistically significant systematic error was found[31]. In all cases, deviation was explained as caused by stochastic dispersion related to subsampling, measurement errors, mechanical disturbance related to taphonomic processes, etc. All these phenomena are included in the uncertainty parameter α_{95}.

Paleomagnetic analyses of the block specimens consisted of the thermal demagnetization of the Natural Remanent Magnetization (NRM) (between 17 and 22 steps from room temperature up to 575-680 °C). Thermal demagnetization was carried out with ASC Model TD48 Thermal Demagnetizers (TD48-SC/TD48-DC). The remanence was measured with a 2G-755 Superconducting Rock magnetometer (noise level $\sim 5\times10^{-12}$ Am^2), using the '2G Enterprises Data Acquisition' software (versions 3.7 and 2.99.5). Thermal demagnetization was preferred because partial thermoremanence (pTRM) is usually the main mechanism of magnetization observed in the thermally altered substrate of this type of materials, as we have also demonstrated experimentally with actualistic fire recreations under controlled conditions[31]. Paleomagnetic results were analyzed using Remasoft 3.0[44]. This analysis involved visual inspection of orthogonal NRM demagnetization diagrams along, with their respective stereograms and intensity decay curves. The Characteristic Remanent Magnetization (ChRM) direction was determined through linear regression. Mean directions and associated statistical parameters were calculated using Fisher's statistics[41] with the assistance of Remasoft.

Thermomagnetic curves (magnetization *vs*. temperature) up to 700 ºC in air were conducted using a Magnetic Measurements' Variable Field Translation Balance (MM_VFTB) to characterize the main carriers of the remanence and assess their thermal stability. Rock magnetic data was collected using the Variable Field Translation Balance software. The results were analyzed with the software RockMag Analyzer 1.1[45].

All the archeomagnetic and rock magnetic experiments were carried out at the laboratory of Paleomagnetism of the University of Burgos in Spain.

Archeostratigraphy & spatial analysis

The main goal of archeostratigraphy is to separate and establish the temporal order of archeological remains found within stratigraphic units. To achieve this, it is necessary to isolate beds of anthropogenic materials based on facies containing them, while also considering the original substrate's topography. This approach allows us to distinguish different paleosurfaces or distinct material inputs within a single facies).

These vertically individualized beds of materials serve as analytical units with higher temporal resolution compared to the broader stratigraphic units (i.e. archeostratigraphic units), which bring us closer to the timescale relevant to human activities [e.g. [21, 46-49]]. Various diachrony markers are taken into account including:

- Archeological material gaps between material beds possibly indicating periods without human occupation, regardless of their duration.

- Archeological materials correlated with the black layers of hearths potentially representing human occupations preceding the combustion event [cf. [19]].

- Hearth ashes or white layers and their associated materials as evidence of human activity contemporaneous with the combustion event and postdating the materials in the underlying black layer. Often, these materials are found at the white-black layer interface, potentially representing a human occupation surface.

We selected archeological materials stratigraphically associated with the white and black layers of the six combustion structures analyzed through archeomagnetism (H34, H48, H50, H55, H57 and H59). This selection included 1,411 faunal remains, 1,496 flint elements, 56 limestone flakes and pebbles, and 122 fragments of thermally altered travertine and tufa.

Anthropogenic material beds identified during fieldwork (Extended data Fig. 5) and tentatively correlated with the hearths were isolated based on sedimentary microtopographic features and stratigraphic relationships among the materials [cf. [37]]. The analysis was conducted separately for the Inner and Outer Part of the site due to (a) a higher number of hearths in the Inner Part, making it easier to distinguish paleosurfaces; (b) thinner sedimentary facies away from the wall, resulting in thicker accumulations in the Inner Part; and (c) greater sedimentary facies complexity in the Inner Part. Outer Beds 2 to 5 correlate with Inner Beds 2-5.1 and 2-5.2, Outer Beds 6 and 7 correlate with Inner Beds 6-7.1 to 6-7.5, and Outer Beds 8 to 10 correlate with Inner Beds 8-10 (Extended data Fig. 5).

Materials included for georeferencing were all flint items, every limestone flake and pebble, bones remains longer or wider than 1 cm and those shorter or narrower but displaying any recognizable anatomical part. Additionally, fragments of burnt travertine or tufa larger than 5 cm were included.

The three-dimensional coordinates of hearth surface areas and perimeters and faunal and lithic elements were recorded using Sokkia® iM-50 Series and Leica® FlexLine TS-02 total stations, along with their standard software. Georeferenced points were plotted two and three-dimensionally using geographic information systems (GIS) software, such as Environmental Systems Research Institute® (ESRI) ArcGIS Desktop ArcMap and ArcScene, versions 10.2.2 and 10.5 for both.

Data availability statement

Archaeomagnetic dataset is available at MagIC database (DOI: 10.7288/V4/MAGIC/20054). Archeostratigraphic data is included in the main figures, Extended Data figures and Supplementary Note 2.

Code availability statement

The program designed for the temporal calculations is available at https://doi.org/10.5281/zenodo.10931465 and at http://pc213fis.fis.ucm.es/program.html.

Methods references:

43. Á. Carrancho, J. J. Villalaín, J. M. Vergès, J. Vallverdú, Assessing post-depositional processes in archaeological cave fires through the analysis of archaeomagnetic vectors. Quaternary International 275, 14-22 (2012).

44. M. Chadima, F. Hrouda, Remasoft 3.0 – a user-friendly paleomagnetic data browser and analyzer. Travaux Géophysiques XXVII, 20–21 (2006).

45. R. Leonhardt, Analyzing rock magnetic measurements: the RockMagAnalyzer 1.0 software. Computers & Geosciences 32, 1420–1431 (2006).

46. A. Bargalló, M. J. Gabucio, F. Rivals, Puzzling out a palimpsest: testing an interdisciplinary study in level O of Abric Romaní. Quaternay International 417, 51-65 (2016).

47. J. Machado, C.M. Hernández, C. Mallol, B. Galván, Lithic production, site formation and Middle Palaeolithic palimpsest analysis: in search of human occupation episodes at Abric del Pastor stratigraphic unit IV (Alicante, Spain). Journal of Archaeological Science 40, 2254-2273 (2013).

48. J. Machado, A. Mayor, C.M. Hernández, B. Galván, Lithic refitting and the analysis of Middle Palaeolithic settlement dynamics: a high-temporal resolution example from El Pastor rock shelter (eastern Iberia). Archaeological and Anthropological Sciences 11, 4539-4554 (2019).

49. V. Spagnolo, G. Marciani, D. Aureli, I. Martini, P. Boscato, F. Boschin, A. Ronchitelli, Climbing the time to see Neandertal behaviour's continuity and discontinuity: SU 11 of the Oscurusciuto rockshelter (Ginosa, southern Italy). Archaeological Anthropological Sciences 12, 1-30 (2020).

Acknowledgments:

Thanks are given to Juan Antonio Espinosa for his help during the first sampling season in 2014 and to all the persons who participated in the excavation seasons. Thanks are also given to Ada Dinckal for his advice. AHL thanks the financial support of the Junta de Castilla y León & the European Regional Development Fund (postdoctoral contract; project BU037P23), the Spanish Ministry of University & European Union-NextGenerationEU (Margarita Salas grants; 2022-2024) and Junta de Castilla y León & European Social Fund, (Predoctoral contracts' program - ORDEN EDU/310/2015, de 10 de abril; 2015-2019). SSR thanks the support of a Generalitat Valenciana predoctoral contract (ACIF/2021/407; 2021-2025). AM thanks the support of a Universitat d'Alacant predoctoral contract (UAFPU2018-049; 2019-2022). MSSB thanks the support of the contract CT36/22-16-UCM-INV (European Union-Next Generation EU). The support of the projects HAR2015-68321-P and CGL2016-77560-C2 (Spanish Ministry of Economy and Competitiveness & European Regional Development Fund), BU235P18 (Junta de Castilla y León & European Regional Development Fund), BU037P23 (Junta de Castilla y León and the European Regional Development Fund), PID2019-107113RB-I00, PID2019-105796GB-I00, PID2019-108753GB-C21 and PID2020-113316GB-I00 (Agencia Estatal de Investigación, Spain; AEI /10.13039/501100011033), PALEOCHAR–648871 (ERC Consolidator Grant), and

Neandertal Fire Technology Project (The Leakey Foundation, Neandertal Fire Technology Project) is also appreciated.

Author contributions:

AHL, AC and JJV performed the conceptualization, archeomagnetic sampling and archeomagnetic analyses and their interpretation. FJPC and MSSB developed and carried out the statistical procedures for the temporal estimations based on archeomagnetic data. AM, SSR and CMH developed the archeostratigraphic and spatial analyses. CM, CMH and BG directed the excavation at El Salt. AHL, AM, SSR, AC, JJV, CM, CMH, FJPC, MSSB wrote and reviewed the paper with contributions of all authors.

Competing interests: Authors declare that they have no competing interests.

Supplementary Information is available for this paper.

Correspondence and requests for materials should be addressed to Ángela Herrejón Lagunilla.

Extended data

Extended data Fig. 1. **(A)** General view of El Salt, with the travertine wall on the right. **(B)** View of the surrounding area of El Salt [yellow star indicates the location of the archeological site]. **(C)** Plan drawing of El Salt site. The materials studied here are from the Lower Excavation Area.

Extended data Fig. 2. Section of the hearth H55, where the typical stratigraphy of this type of structure is observed (white layer at the top, black layer at the base).

Extended data Fig. 3. Representative image of an excavation surface within Unit X at the Inner Part of El Salt, with a visible complexity of sedimentary facies, hearths and abundant archeological materials (marked with color pins).

Extended data Fig. 4. General archeostratigraphic log of Unit X_b based on excavation and field observations, showing the stratigraphic relationships among combustion structures and material beds (Hearths selected for this study in bold).

Extended data Fig. 5. Archeostratigraphic scheme showing the relationships among the material beds associated with the hearths included in this study.

Extended data Fig. 6. Thermomagnetic curves of representative samples of white (a-c) and black layers (d-f) from the studied hearths. Paramagnetic correction was applied in all cases. Red and blue lines indicate the heating and cooling cycles, respectively. This experiment was performed on 11 different representative samples.

Extended data Fig. 7. Equal area projections of the studied hearths showing the mean archeomagnetic directions related to the last combustion event and their respective circle of confidence at 95% probability [$p = 0.05$] or α_{95} (pink symbols) and the ChRM direction calculated from each specimen (black symbols represent downward inclination). From left to right, starting with the top row: H34 (16 specimens from 2 oriented blocks), H57 (5 specimens from 1 oriented block), H55 (21 specimens from 4 oriented blocks), H48 (7 specimens from 1 oriented block), H59 (8 specimens from 1 oriented block), H50 (9 specimens from 1 oriented block). Calculations are based on Fisher's statistics[41]. Statistical details are shown in Table 1. Thermal demagnetization of Natural Remanent Magnetization (NRM) is performed only once on each specimen due to the irreversible character of the experiment (it causes the progressive destruction of the original NRM). For this reason, a minimum of 8 specimens per hearth were demagnetized to obtain directional data. Specimens shown here correspond to those accepted after filtering (Supplementary Methods 1).

Extended data Fig. 8. Orthogonal NRM demagnetization diagrams of some representative specimens and their respective normalized intensity decay plots: A) D1AX1, B) E1BX2, C) C2CX1, D) E4C3X. Solid/open symbols in orthogonal diagrams correspond to the vector endpoints' projections onto the horizontal/vertical plane. These specimens mainly contain thermally altered substrate, although (d) may include traces of ash. NRM values are normalized by the estimation of specimens' mass excluding plaster content. Steps below 200 ºC were disregarded to avoid any viscous influence.

Extended data Fig. 9. (a) Representative example of orthogonal NRM demagnetization diagram of a specimen from block C1 (white layer from H50) and its respective normalized intensity decay plot. Symbols as in Extended data Fig. 7. (b) Equal area projection of the mean direction of ChRM (related to the burning event), along with their respective α_{95} (circle of confidence at 95% probability; $p = 0.05$), calculated with specimens from block C1 (red; 9 specimens from 1 oriented block; $k = 133.2$; $\alpha_{95} = 4.5º$) *vs*. direction calculated with H50 specimens selected for the final direction (blue; 9 specimens from 1 oriented block; $k = 105.9$; $\alpha_{95} = 5.0º$). Directions for individual specimens are also shown (green symbols = C1 block specimens; black symbols = specimens accepted for H50 final direction). C1 specimens are affected by flattening (see Supplementary Methods 1). Solid symbols represent downward inclination. NRM values are normalized by the estimation of specimens' mass excluding plaster content. [WL = White Layer]. Calculations of mean directions are based on Fisher's statistics[41]. Thermal demagnetization of Natural Remanent Magnetization (NRM) is performed only once on each specimen due to the irreversible character of the experiment (it causes the progressive destruction of the original NRM). For this reason, a minimum of 8 specimens per hearth were demagnetized to obtain directional data. Specimens shown here correspond to those accepted after filtering (Supplementary Methods 1).

Extended data Table 1. Estimation of the time elapsed between fires (Δt_{min}) according to the different reconstructions. From left to right: pair of hearths (column 1), reconstruction (column 2) and estimated minimum elapsed times (columns 4-6). The estimated minimum elapsed time (Δt_{min}) is given at four different statistical levels (mode, column 3; 99%: column 4; 95%, column 5; 68%, column 6).

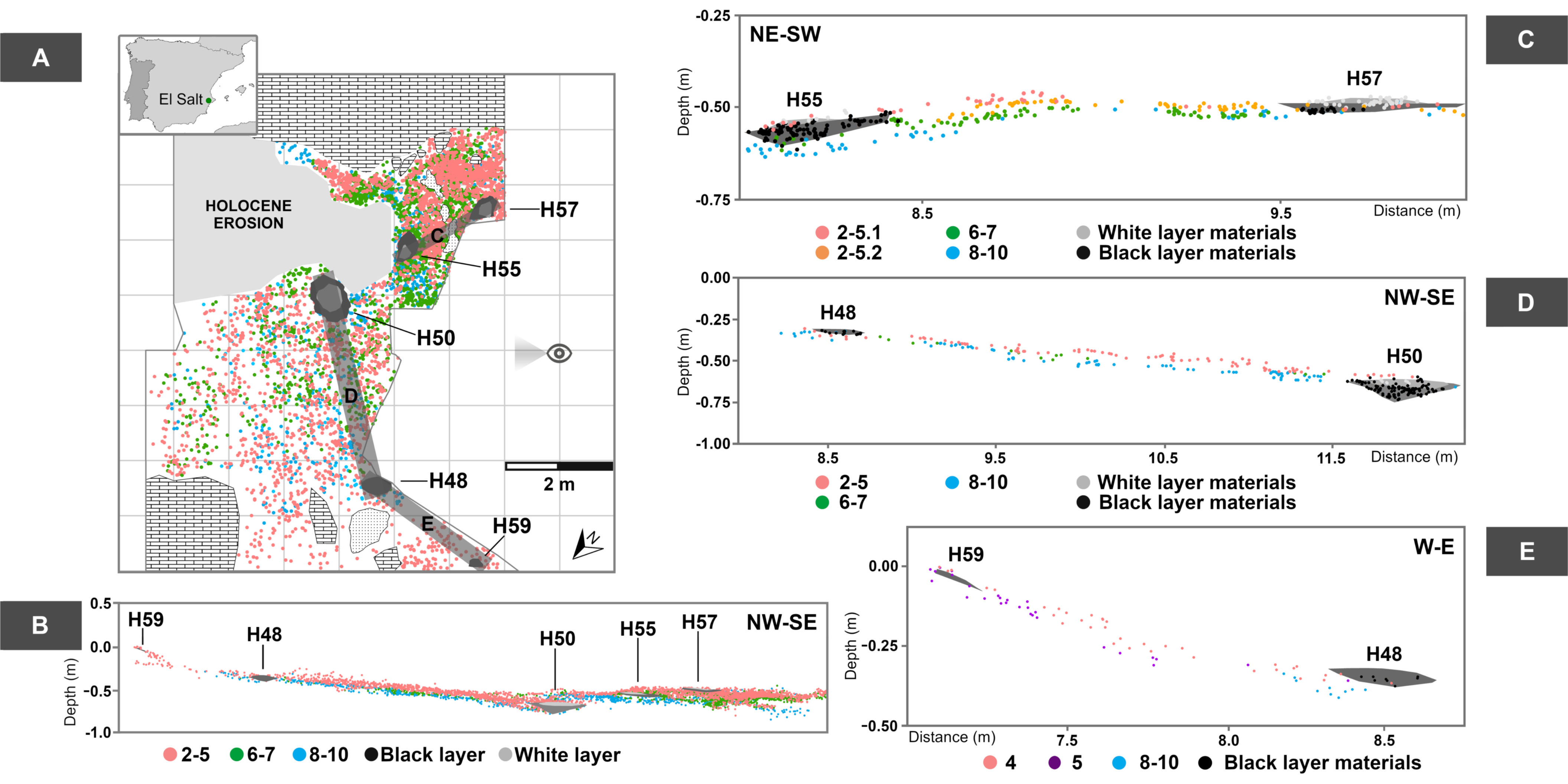

A
El Salt
HOLOCENE EROSION
H57
C
H55
H50
D
H48
E
H59
2 m
N
B
H59
H48
H50
H55
H57
NW-SE
0.5
0.0
-0.5
-1.0
Depth (m)
2-5
6-7
8-10
Black layer
White layer
C
NE-SW
H55
H57
-0.25
-0.50
-0.75
Depth (m)
8.5
9.5
Distance (m)
2-5.1
2-5.2
6-7
8-10
White layer materials
Black layer materials
D
NW-SE
H48
H50
0.00
-0.25
-0.50
-0.75
-1.00
Depth (m)
8.5
9.5
10.5
11.5
Distance (m)
2-5
6-7
8-10
White layer materials
Black layer materials
E
W-E
H59
H48
0.00
-0.25
-0.50
Depth (m)
Distance (m)
7.5
8.0
8.5
4
5
8-10
Black layer materials

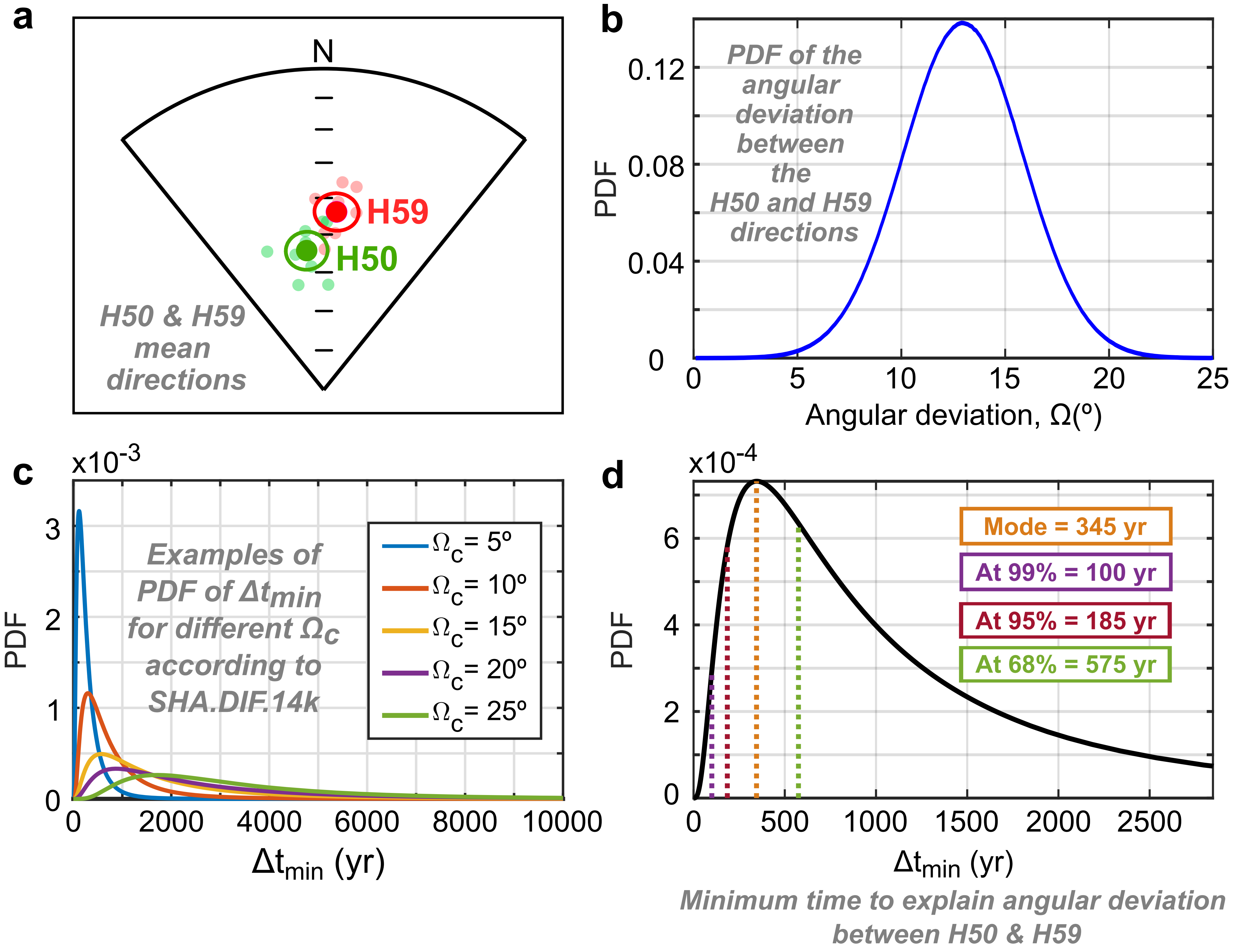

a
N
H59
H50
H50 & H59
mean
directions
b
PDF of the
angular
deviation
between
the
H50 and H59
directions
PDF
0.12
0.08
0.04
0
0
5
10
15
20
25
Angular deviation, Ω(º)
c
x10-3
3
2
1
0
PDF
Examples of
PDF of Δtmin
for different Ωc
according to
SHA.DIF.14k
Ωc= 5º
Ωc= 10º
Ωc= 15º
Ωc= 20º
Ωc= 25º
0
2000
4000
6000
8000
10000
Δtmin (yr)
d
x10-4
6
4
2
0
PDF
Mode = 345 yr
At 99% = 100 yr
At 95% = 185 yr
At 68% = 575 yr
0
500
1000
1500
2000
2500
Δtmin (yr)
Minimum time to explain angular deviation
between H50 & H59

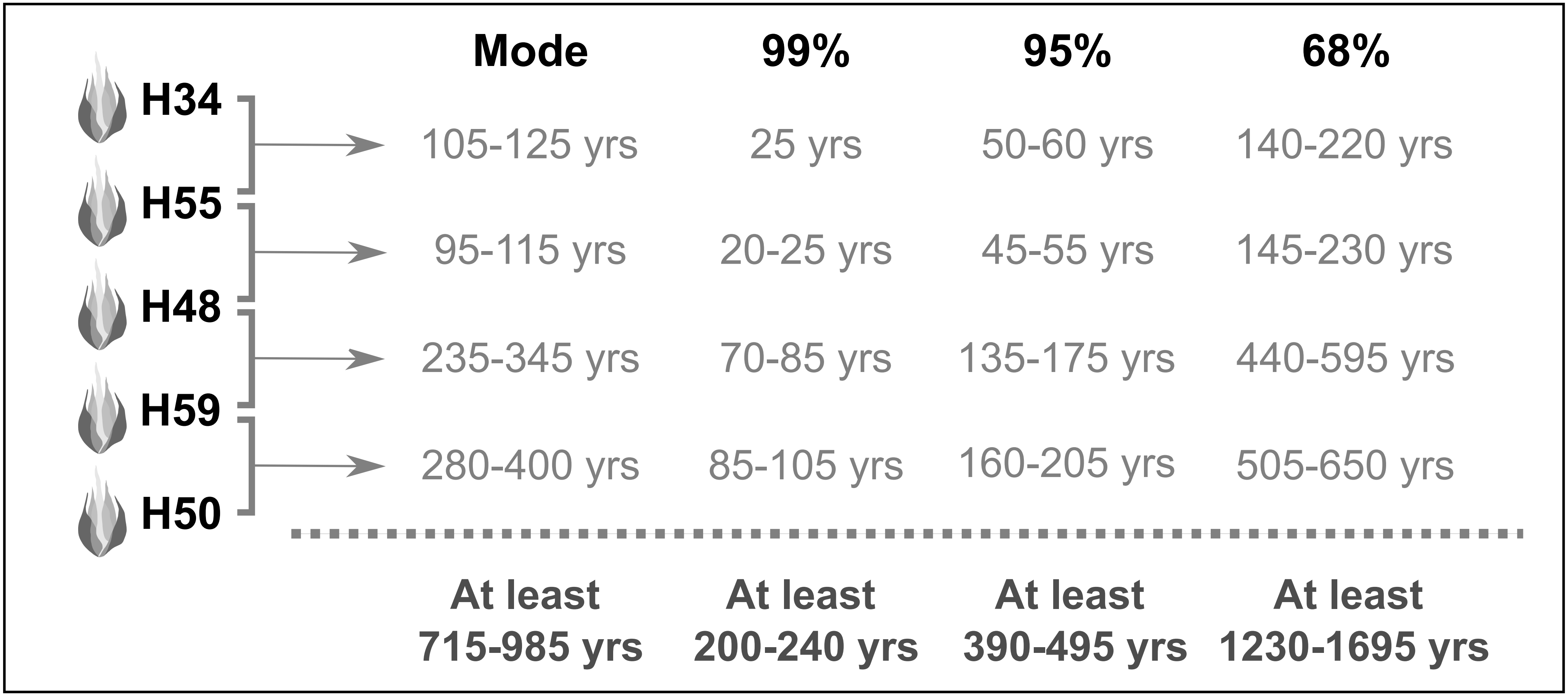
Mode
99%
95%
68%
H34
105-125 yrs
25 yrs
50-60 yrs
140-220 yrs
H55
95-115 yrs
20-25 yrs
45-55 yrs
145-230 yrs
H48
235-345 yrs
70-85 yrs
135-175 yrs
440-595 yrs
H59
280-400 yrs
85-105 yrs
160-205 yrs
505-650 yrs
H50
At least 715-985 yrs
At least 200-240 yrs
At least 390-495 yrs
At least 1230-1695 yrs

Combustion structure	N/N'	Dec. (º)	Inc. (º)	k	α_{95}
H34	16/17	6.6	55.4	97.3	3.8
H57	5/8	358.1	55.0	31.1	13.9
H55	21/30	3.6	49.8	52.2	4.4
H48	7/10	3.5	55.6	77.3	6.9
H59	8/12	4.1	43.7	117.5	5.1
H50	9/10	352.9	54.0	105.9	5.0